ISBN: 978-3-95450-222-6 ISSN: 2673-5350 doi:10.18429/JACoW-IBIC2020-WEA002

THz DETECTION TECHNIQUES OVERVIEW

F. Mazzocchi, D. Strauß, T. Scherer, KIT IAM-AWP, Eggenstein Leopoldshafen, Germany
A. S. Müller, E. Bründermann, KIT IBPT, Eggenstein Leopoldshafen, Germany

Abstract

In the following work, we present a general overview of the various techniques that can be employed to detect and characterize THz waves. The overview will take into consideration several technologies based on different physical principia, capable of both broadband and narrowband detection.

INTRODUCTION

In recent years, the THz part of the electromagnetic spectrum has attracted special attention due to the broad range of possible applications deriving from it and its presence in multiple natural phenomena. T-rays are able to pass almost unobstructed through a wide range of non-polar materials such as fabrics, paper, wood, ceramics, plastics and plasma. Radioastronomy, spectroscopy, molecular sensing, plasma diagnostics, security and biomedical imaging are only a few possible uses of the THz spectrum. Such wide range of applications demands a similarly wide range of detection techniques and devices. The methods presented in this overview have been organized in four groups, based on the physical principia they rely on: thermal, direct, heterodyne and sampling detection. For each of the techniques, the operational limits and the most frequent applications are also presented.

THERMAL DETECTORS

Conceptually speaking, thermal detectors represent the simplest sensors employed for power measurements in the THz region, and can be thought as composed by three distinct parts: the radiation absorber, the heat sink and the thermal link between them (Fig. 1).

Radiation impinging on the absorber determines a rise in temperature $\Theta(T)$ given by [1]

$$\Theta = \frac{\eta P_\omega}{\sqrt{\omega^2 C^2 + G^2}} \tag{1}$$

where C and G are, respectively, the thermal capacity and conductivity. η is the detection efficiency and P_ω the power related to the incoming radiation. We can define the response time of the detector as

$$\tau = C/G \tag{2}$$

that is minimized for small thermal masses and high conductivities. For room temperature detectors, we can expect response time ranging from as few seconds to a few milliseconds. Examples of thermal detectors include pyroelectrics, thermopiles, Golay cells and bolometers. Nowadays, bolometers are the most widespread of these kind of

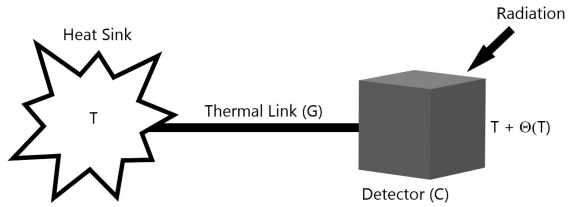

Figure 1: Schematic representation of a thermal detector main elements.

detectors, and will be the main subject of the section. The reader interested in the other aforementioned devices can refer to [1] for a more extensive treatment. In 1961 Low [2] described a popular bolometer based on germanium, that consisted in a doped semiconductor absorber suspended in vacuum by wires that function as both thermal and electrical contacts. The semiconductor is biased with a constant current, and the change in temperature induced by the absorbed radiation determines a detectable change in the electrical resistance of the device. We can introduce the generalized resistance temperature coefficient α as:

$$\alpha = R^{-1}\,(dR/dT) \tag{3}$$

where R and T are the resistance and temperature. α represents the steepness of the R/T curve. Of course the higher the voltage response of the detector to a given signal, the better. This is achieved by cooling the device down to liquid helium temperatures or lower. The obtained reduced thermal capacitance determines therefore a faster and more sensitive detector. Given that bolometers are operated with a current bias, there is an additional varying electrical power that leads to an effective thermal time constant $G_{Eff} = G - \alpha P_E = G - I^2 R\alpha$. Semiconductor bolometers typically require heavy doping, in order for them to have a more metal like behaviour of the resistance, avoiding thermal runaways. The main conduction mechanism is, in this case, performed by charge carriers passing from one donor atom to the other. The resistance temperature coefficient takes the explicit form of

$$\alpha = -\frac{1}{2}\sqrt{\frac{T_0}{T^3}} \tag{4}$$

with T_0 in the order of 2–10 K. Semiconductor bolometers can reach Noise Equivalent Power (NEP) in the order of 10^{-12}–10^{-13} W/Hz$^{1/2}$ in a 0.15–15 THz frequency range and response times of roughly 10 µs. Applications in astrophysics are the most widespread, with notable instru-

ISBN: 978-3-95450-222-6 ISSN: 2673-5350 doi:10.18429/JACoW-IBIC2020-WEA002

ments like SPIRE [3] in the Herschel Space Observatory and SCUBA [4] inside the Maxwell Mauna Kea Observatory.

Higher sensitivities in bolometers can be achieved by taking advantage of the very narrow superconducting transitions. Materials like tantalum [5], niobium nitride [6] and niobium [7] are regularly used in the form of superconducting thin films in such devices. Since they have a positive temperature coefficient, they require a constant voltage bias instead of a constant current, in order to avoid thermal runaways. When the voltage is kept constant, absorbed radiation power determines a decrease of the bias current (electrothermal feedback), that cannot therefore exceed the limit $G_{Eff} = 0$ that determines the runaway. Since with these devices we tend to work close to the superconducting transition, where the R/T curve is steeper, they are commonly referred also as Transition Edge Sensors (TES). They reach extremely small NEP values, around 10^{-19} W/Hz$^{1/2}$ at $10^{-15} W$ of background illumination [8] and response times in the order of microseconds. SCUBA2 [9] is an example of instrument using such detectors. For the detection of low energy photons, typically below 1.5 THz, lower effective mass carriers are needed in order to be sensitive to lower ionization levels. Hot Electron Bolometers [10] (HEBs) also require the use of superconductors. At cryogenic temperatures, the electrons are only weakly coupled with the phonon system and even small energies can break this bond, generating the hot electrons referred by the device's name. The phonons of the thin film represent the thermal reservoir of the bolometer, and the heat capacitance involved in the detection mechanism is the one of the electrons. The electron phonon relaxation time represents, therefore, the relevant thermal conductance of the whole system. HEBs are typically capable of NEPs in the order of 10^{-18} W/Hz$^{1/2}$ and response time around the 10 ps range, making them adapt to detecting the bunch dynamics of a synchrotron storage ring.

DIRECT DETECTORS

Direct detectors include a large range of very different devices, including rectifiers, superconducting vortex assisted and kinetic inductance detectors, to name a few. Schottky diodes are the most prominent examples of the rectifiers family. In such devices, the impinging electro-magnetic radiation acting on the sensor induces an AC at the radiation frequency and, given a non linear voltage - current curve of the device, a DC component rises, that is related to the amplitude of the input. The Schottky barrier [11] is formed by the junction of a metal with a semiconductor, and presents a very low forward voltage drop when compared to other kind of diodes. This aspect, together with the fact that Schottky diodes are majority carrier devices, allows for very fast switching, with time constants lower than 10 ps. They can be operated at room temperature and bias free, which limits the noise level. Typical zero-bias NEP values are in the 10^{-12} W/Hz$^{1/2}$ range. Recent development in the fabrication techniques have allowed very wide band devices, with the detectable frequencies range as wide as 50 GHz–5 THz. They are regularly employed, as an example, in microbunching measurements [12], where time resolutions in the order of a nanosecond are required. Another device pertaining to the family of rectifiers is the Superconducting Tunnel Junction (STJ), also know as superconductor-insulator-superconductor (SIS) tunnel junction. As the name suggests, it consists of twin layers of superconductors separated by a very thin (around tens of Angstrom) insulator membranes. When cooled down below their critical temperature, Cooper pairs start to form, with binding energy 2Δ that is also the gap of the density of states. The gap voltage is defined as:

$$V_G = \frac{2\Delta}{e} \tag{5}$$

A bias voltage equal to the gap voltage will make the densities of states at both sides of the insulator to overlap, and Cooper pairs will break down back to single electrons. These quasiparticles can tunnel through the insulating barrier, if it is thin enough, and recombine into Cooper pairs on the other side of it. This results in a steep increase of current in the I-V curve of the device. During normal operation, the DC bias will be kept below the gap limit, and incoming photons will break down Cooper pairs into normal electrons, that then tunnel through the barrier in the direction of the applied voltage. The tunnelling current is proportional to the energy of the photons, since more energetic quanta will generate more quasiparticles. Devices of these kind dedicated to photons detection in the submillimeter range operate mostly between 0.7 and 2.4 THz, with NEPs in the order of 10^{-18} W/Hz$^{1/2}$ at 1 THz [13]. They are extensively used in the astrophysics field as single photon detectors in a wide range of frequencies, from IR to X-rays. Another technology that has been first developed in the astrophysics [14] field and that is being adapted only recently to other applications, such as fusion plasma diagnostics [15], is the Kinetic Inductance Detector, or KID. Such a device consists of an array of superconducting microresonators, each with a natural resonance frequency equal to

$$\nu_R = \frac{1}{\sqrt{LC}} \tag{6}$$

with L and C representing the inductance and capacitance of the resonator. The kinetic inductance derives from the inertial mass of the charge carriers (again a mixture of Cooper pairs and electrons) when they are subject to high frequency alternating electrical fields. Photons striking the detector can break down Cooper pairs if their energy is bigger than the 2Δ gap, generating quasi particles. At this point, the kinetic part of the microresonator inductance increases, resulting in a shift of the complex scattering transmission parameter S_{21} peak toward lower frequency values, in addition to a change in phase. One of the biggest advantages of this technology is the ease with which it can be read out. By tuning each microresonator to a unique resonance, arrays of hundreds of pixels can be easily multiplexed with a single feed line, either a microstrip or a co-planar waveguide.

ISBN: 978-3-95450-222-6 ISSN: 2673-5350 doi:10.18429/JACoW-IBIC2020-WEA002

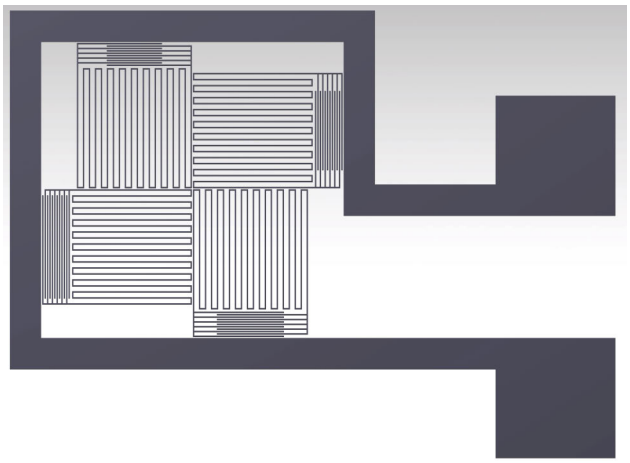

Figure 2: 2D model of the KID array developed as polarimetric fusion plasma diagnostic at KIT IAM-AWP [15]. The pixels are two by two sensitive to only one plane of polarization, in virtue of their orientation. The meandering line of each resonator represents their inductance L and it's the same for all the pixels, while the capacitors are different in number and length of their digit to tune the resonance frequency.

Additionally, the fabrication is very simple, since only single layer deposition is needed and photolithography allows very fast production times. The detectors used in astrophysics are normally made of aluminium thin films (T_C = 1.2 K) and operated in the 250–300 mK range. The use of superconductors with higher critical temperatures like niobium and niobium nitride, with T_C in the 9–15 K range, allows the use of normal liquid He cryostats instead of more expensive closed refrigerators system, at the cost of a reduced sensitivity. These detectors can easily reach values of 10^{-18} W/Hz$^{1/2}$ for the NEP, with record values toward 10^{-19} W/Hz$^{1/2}$ [16], maximum energy resolution of 100 meV and a rise time around 50 ps. The bandwidth can be tuned to cover detection from the radiofrequency range up to the X-rays, and they can be made intrinsically polarization sensitive. The instrument NIKA2 [17] is a good application example of such technology.

Most of the detectors treated so far require cooling down to liquid helium temperatures or even below, to guarantee their optimal operation. While LHe cryogenic techniques are well developed and reliable, they add a degree of complexity to the systems equipped with these technologies. Additionally, few of them reach the required response time to fully resolve, for example, the dynamics of a storage ring bunch. With these premises in mind, an innovative device in the form of a high temperature superconductor detector has been recently developed for measurements at the Karlsruhe Research Accelerator (KARA). It consists of microbridges of $YBa_2Cu_3O_7$ (or YBCO) from 30 nm thick films [18] on a R-cut sapphire substrate. YBCO has a T_C of around 83 K, making the use of liquid nitrogen temperatures feasible. The fast (< 15 ps) photoresponse of these detectors at THz ranges has been demonstrated to be vortex-assisted rather than bolometric in nature [19]. Type II superconductors are characterized by the formation of what are called Abriksov vortices, especially when an external magnetic field is applied to it. These vortices are composed by supercurrent loops circulating around a non superconducting core, and are therefore sensitive to electric and magnetic fields. The electric field from a storage ring generates a current pulse across the microbridge. This pulse causes the vortices to rearrange in a line, creating a channel that facilitates the crossing of the bridge. One interesting aspect of this innovative device is that in virtue of the detecting mechanism, it can be operated bias free, simplifying the experimental setup. Additionally, it has a very high responsivity (700 V/W), enabling it to be embedded directly into an ultra fast readout system like KAPTURE [20] without the use of an amplifier.

HETERODYNE DETECTION

Heterodyne detection is an extremely widespread technique, since it is at the base of modern day TV, Radio and wireless telecommunication. Two signals of similar frequency that coexist in the same circuit will generate additional frequencies determined by their sum and difference. The receiver is optimized for the detection of the difference frequency, since it's value is orders of magnitudes (GHz for THz signals) lower than the beat frequency. Such a receiver can be divided into two main building blocks: front and back end. The front end is responsible for the collection of the THz radiation, while the back end task is to collect the signal from the front end, to amplify it and to detect it. The front end itself contains two main elements, in the form of a Local Oscillator (LO) and a mixer. The local oscillator is responsible for the generation of the reference signal to be subtracted to the incoming radiation, and at THz ranges can take the form of multiplied microwave emitters for frequencies below 2 THz, or Quantum Cascade Lasers (QCLs) at shorter wavelengths. The generation of the additional frequencies is then performed in the mixer, a nonlinear electrical circuit. The nonlinearity is a required characteristic, since the additional frequencies are generated by the higher order terms of the expansion of the I-V curve:

$$I(V) = k_0 + k_1 V + k_2 V^2 + \cdots = \sum_{i=0}^{\infty} k_i V^i \qquad (7)$$

given an input voltage of the form:

$$V = V_{LO} \sin(\omega_{LO} t) + V_S \sin(\omega_s t) \qquad (8)$$

The power of the harmonics decreases with the square of the harmonic number, therefore only the sum and difference (or intermediate frequency ν_{IF}) are transferred to the back end in a significative quantity, in the case of double sideband (DSB) mixers. The mechanism described above is proper of the so called square law mixers, since the device responds to the square of the sum of the waveforms fields. If the mixer was to react individually to the signals, then it would function more as a switch, acting on the voltage waveform

ISBN: 978-3-95450-222-6 ISSN: 2673-5350 doi:10.18429/JACoW-IBIC2020-WEA002

induced by the LO field, with his action dictated by the radiation signal. The resulting output in this case is the product of the switching and signal waveform, and, when its duty cycle is not 50%, contains all the superior harmonics that therefore need to be filtered out. Slow mixers with detection mechanism unable to follow the fast dynamics of the fields, respond to the total power of the incoming radiation and fall into the first category that includes the hot electron bolometers. Fast devices like the Schottky diode or the SIS junctions can be used as switching mixers. In heterodyne detection, a good indication of the noise level of the device is given by the receiver noise temperature T_{REC} that in the end determines the sensitivity of the device, the minimum detectable power in a given integration time:

$$\Delta T_{MIN} = \frac{k_{REC} T_{REC}}{\sqrt{\tau \Delta \nu}} \tag{9}$$

where k_{REC} is a receiver dependent constant, $\Delta\nu$ is the detection bandwidth and τ the integration time. Generally speaking, Schottky diodes present higher noise figures compared both HEBs and SIS mixers (Fig. 3), and the noise temperature raises for higher frequencies. Heterodyne systems are widely used, as an example, in the Electron Cyclotron Emission (ECE) diagnostics installed in nuclear fusion machines, like Wendelstein 7X [21], to determine the electron temperature. It consists of a 32 channel radiometer, capable of covering the second harmonic of the ECE, in a range from 126 to 160 GHz, donwnconverting it to 4–40 GHz. There's a notch filter installed at 140 GHz, since the Electron Cyclotron Resonance Heating (ECRH) system operates at that frequency and would overload the radiometer if its radiation was allowed to pass through. Each of the 32 channels refers to a precise flux surface (constant magnetic field) of the plasma, since the emission frequency is dependent on the magnetic field strength that itself is a function of the radial coordinate inside the toroidal vacuum chamber. The radiometer uses a single broadband diode mixer and a local oscillator at 122 GHz [22].

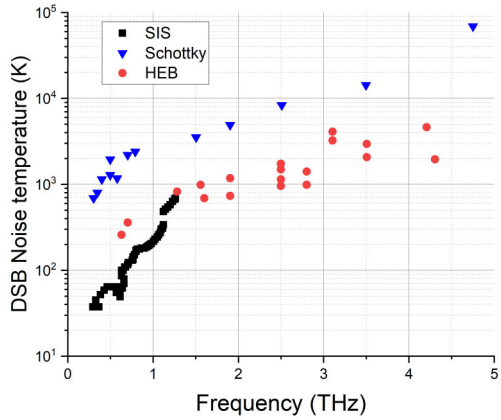

Figure 3: Noise figures for different kind of mixers. Data extracted from Fig. 5.35 in Ref. [1].

SAMPLING DETECTION

The development of fs-lasers in the last 25 years led, among other things, to advancement in both generation and detection of THz radiation. Sampling detection uses either a gated photoconductive antenna (Auston Switch [23]) or non linear optical crystal like ZnTe (Electro Optical Sampling, EOS [24]) to sample and extract information from a THz pulse. In the first of these techniques, light from the fs-laser impinges on the antenna, exciting the charge carriers. The conductivity changes abruptly, supported by the newly photogenerated electrons. The incoming THz radiation act as a voltage bias, driving a current in the antenna. Since the fs pulse is much shorter than the THz one, the change in conductivity can be considered as a delta function, and the induced current has the same pulse shape as the THz electrical field [1]. Electro Optical Sampling is based on the Pockels effect present in many crystals that lack inversion symmetry, like ZnTe [25]. These crystals show birefringency when a voltage is present across their section. The magnitude of the difference between the ordinary and extraordinary refractive indices depends linearly on the magnitude of the electric field, therefore this phenomenon is also known as linear electro-optical effect. In this frame, the THz radiation acts as modulation signal for the crystal, changing the birefringency according to its pulse shape. A concurrent ultrafast fs-laser pulse will see its polarization status modified accordingly with the temporal profile of the modulation. At this point, a Wollaston prism is used to separate the extraordinary and ordinary components of the fs pulse with the encoded information, each one impinging on a separate balanced detector. The difference in signal between the P and S detectors allows to reconstruct the amplitude of the THz waveform. Both techniques are widely employed in Time Domain Spectroscopy (TDS) [26], that consists in a pump-probe kind of technique where the pump signal is used to generate the THz radiation and the probe signal to gate the detector or modulate the polarization status of the THz pulse to be detected. The generation methods mirror the detection ones, with, respectively, photoemission from a voltage biased antenna or optical rectification by a non linear crystal [27]. Auston switch-based systems are limited by the parameters of the antenna to, typically, a maximum of 6 THz although recently bandwidths in excess of 70 THz have been achieved [28] through Au-implanted Ge emitters. The antenna structure, together with the materials properties determine also the response time, that can be around 300 fs with InGaAs emitters [29]. In EOS, the bandwidth is limited mainly by the length of the fs pulse and by the thickness and the absorption of the crystal. It can have an extreme extension, from 100 GHz to 37 THz [30]. As an example, EOS has been employed as longitudinal diagnostics for single-shot electron bunch profiling at the KARA facility in Karlsruhe [31]. Strong THz radiation bursts can be produced by short electron bunches [32] as result of in-

ISBN: 978-3-95450-222-6 ISSN: 2673-5350 doi:10.18429/JACoW-IBIC2020-WEA002

stabilities patterning. The bunch length was in the order of few picoseconds, with a repetition rate of 2.72 MHz. The laser pulse itself is stretched from femtoseconds length up to picoseconds through a fiber optics stretcher and a compressor, to make it overlap with the bunch pulse and allow single shot acquisition. The electro optical crystal is made out from gallium phosphide. At the end of the system, an ultrafast Si photodiode detector array (KALYPSO [33]) with the repetition rate also set at 2.72 MHz, extracts the encoded bunch profiles on a turn by turn basis.

CONCLUSION

We presented a review of several techniques that can be employed in the field of THz waves detections. The devices presented have been divided into four main categories, spanning from thermal detectors, to direct detection methods, to heterodyne and finally sampling detection. The most sensitive room temperature detector is the normal bolometer, closely followed by the Schottky diode. The latter gains an edge on the former in response time thanks to its very fast switching action. If noise level is a priority, then the superconducting devices here presented present absolutely the best performances, with NEPs for KIDs, HEBs and TES reaching the 10^{-18}–10^{-19} W/Hz$^{1/2}$. Heterodyne systems are capable of extremely wide dynamic ranges (above 100 dB) and present also very good noise figures, especially when equipped with a cryogenic mixer like STJs. Electro optical sampling systems offer an extremely wide bandwidth and the single shot measurement capability, but require very precise synchronization and overlap with the THz pulse.

REFERENCES

[1] E. Bründermann *et al.*, *Terahertz Techniques*, Berlin, Germany: Springer-Verlag Berlin Heidelberg, 2012. doi:10.1007/978-3-642-02592-1

[2] , F. J. Low, "Low-Temperature Germanium Bolometer", *J. Opt. Soc. Am.*, vol. 51, p. 1300, 1961. doi:10.1364/josa.51.001300

[3] M. J. Griffin *et al.*, "The Herschel-SPIRE instrument and its in-flight performance", *A&A*, vol. 518, p. L3, 2010. doi:10.1051/0004-6361/201014519

[4] W. S. Holland *et al.*, "SCUBA: a common-user submillimetre camera operating on the James Clerk Maxwell Telescope", *Mon. Not. R. Astron. Soc.*, vol. 303, pp. 659–672, 1999. doi:10.1046/j.1365-8711.1999.02111.x

[5] A. Skalare *et al.*, "Speed measurements of diffusion-cooled tantalum bolometers", *IEEE Trans. Appl. Supercond.*, vol. 13, pp. 160–163, 2003. doi:10.1109/TASC.2003.813670

[6] R. Romestain *et al.*, "Fabrication of a superconducting niobium nitride hot electron bolometer for single-photon counting", *New J. Phys.*, vol. 6, p. 129, 2004. doi:10.1088/1367-2630/6/1/129

[7] D. F. Santavicca *et al.*, "Antenna Coupled Niobium Bolometers for Terahertz Spectroscopy", *IEEE Trans. Appl. Supercond.*, vol. 17, pp. 412–415, 2007. doi:10.1109/TASC.2007.898191

[8] A. J. Miller *et al.*, "Demonstration of a low-noise near-infrared photon counter with multiphoton discrimination", *Appl. Phys. Lett.*, vol. 83, pp. 791–793, 2003. doi:10.1063/1.1596723

[9] W. S. Holland *et al.*, "SCUBA-2: the 10 000 pixel bolometer camera on the James Clerk Maxwell Telescope", *Mon. Not. R. Astron. Soc.*, vol. 430, pp. 2513–2533, 2013. doi:10.1093/mnras/sts612

[10] F. C. Wellstood *et al.*, "Hot-electron effects in metals", *Phys. Rev. B*, vol. 49, pp. 5942–5955, 1994. doi:10.1103/physrevb.49.5942

[11] R. T. Tung, "The physics and chemistry of the Schottky barrier height", *Appl. Phys. Rev.*, vol. 1, p. 011304, 2014. doi:10.1063/1.4858400

[12] M. Brosi *et al.*, "Fast mapping of terahertz bursting thresholds and characteristics at synchrotron light sources", *Phys. Rev. Accel. Beams*, vol. 19, p. 110701, 2016. doi:10.1103/PhysRevAccelBeams.19.110701

[13] S. Ariyoshi *et al.*, "Terahertz detector based on a superconducting tunnel junction coupled to a thin superconductor film", *Appl. Phys. Lett.*, vol. 95, p. 193504, 2009. doi:10.1063/1.3263711

[14] S. Doyle *et al.*, "Lumped Element Kinetic Inductance Detectors", *J. Low Temp. Phys.*, vol. 151, pp. 530–536, 2008. doi:10.1007/s10909-007-9685-2

[15] F. Mazzocchi *et al.*, "THz multi-line of sight polarimeter for fusion reactors", *Fusion Eng. Des.*, vol. 130, pp. 1–5, 2018. doi:10.1016/j.fusengdes.2018.02.089

[16] P. de Visser *et al.*, "Fluctuations in the electron system of a superconductor exposed to a photon flux", *Nat. Commun.*, vol. 5, p. 3130, 2014. doi:10.1038/ncomms4130

[17] M. Calvo *et al.*, "The NIKA2 Instrument, A Dual-Band Kilopixel KID Array for Millimetric Astronomy", *J. Low Temp. Phys.*, vol. 184, pp. 816–823, 2016. doi:10.1007/s10909-016-1582-0

[18] P. Thoma *et al.*, "Highly Responsive Y–Ba–Cu–O Thin Film THz Detectors With Picosecond Time Resolution", *IEEE Trans. Appl. Supercond.*, vol. 23, p. 2400206, 2013. doi:10.1109/TASC.2012.2233851

[19] P. Probst*et al.*, "Nonthermal response of Y–Ba_2–Cu_3–O_7 thin films to picosecond THz pulses", *Phys. Rev. B*, vol. 85, p. 174511, 2012. doi:10.1103/PhysRevB.85.174511

[20] M. Caselle *et al.*, "KAPTURE-2. A picosecond sampling system for individual THz pulses with high repetition rate", *JINST*, vol. 12, p. C01040, 2017. 10.1088/1748-0221/12/01/C01040

[21] S. Schmuck *et al.*, "Design of the ECE diagnostic at Wendelstein 7-X", *Fusion. Eng. Des.*, vol. 84, pp. 1739–1743, 2009. doi:10.1016/j.fusengdes.2008.12.094.

[22] J. Nührenberg*et al.*, "Overview on Wendelstein 7-X Theory", *Fusion Technol.*, vol. 27, pp. 71–78, 1995. doi:10.13182/FST95-A11947048

[23] B. Di Bartolo and O. Forte (Eds.), "Advances in Spectroscopy for Lasers and Sensing". Netherlands: Springer Netherlands, 2006. doi:10.1007/1-4020-4789-4

[24] B. Pradarutti *et al.*, "Electrooptical sampling of ultra-short THz pulses by fs-laser pulses at 1060 nm", *Appl. Phys. B*, vol. 85, pp. 59-–62, 2006. doi:10.1007/s00340-006-2303-1

ISBN: 978-3-95450-222-6 ISSN: 2673-5350 doi:10.18429/JACoW-IBIC2020-WEA002

[25] J-P. Caumes*et al.*, "Kerr-Like Nonlinearity Induced via Terahertz Generation and the Electro-Optical Effect in Zinc Blende Crystals", *Phys. Rev. Lett.*, vol. 89, p. 047401, 2002. doi:10.1103/PhysRevLett.89.047401

[26] M. Hangyo *et al.*, "Terahertz Time-Domain Spectroscopy of Solids: a Review", *Int. J. Infrared Millimeter Waves*, vol. 26, pp. 1661-–1690, 2005. doi:10.1007/s10762-005-0288-1

[27] A. Rice *et al.*, "Terahertz optical rectification from 110 zinc-blende crystals", *Appl. Phys. Lett.*, vol. 64, pp. 1324–1326, 1994.

[28] A. Singh *et al.*, "Up to 70 THz bandwidth from an implanted Ge photoconductive antenna excited by a femtosecond Er:fibre laser", *Light Sci. Appl.*, vol. 9, p. 30, 2020. doi:10.1038/s41377-020-0265-4

[29] E. R. Brown *et al.*, "State-of-the-art in 1.55 μm ultrafast InGaAs photoconductors, and the use of signal-processing techniques to extract the photocarrier lifetime", *Semicond. Sci. Technol.*, vol. 20, pp. S199–S204, 2005. doi:10.1088/0268-1242/20/7/009

[30] P. Y. Han *et al.*, "Coherent, broadband midinfrared terahertz beam sensors", *Appl. Phys. Lett.*, vol. 73, pp. 3049–3051, 1998. doi:10.1063/1.122668

[31] S. Funkner *et al.*, " Revealing the dynamics of ultrarelativistic non-equilibrium many-electron systems with phase space tomography", 2019. arXiv:1912.01323

[32] E. Roussel *et al.*, "Observing microscopic structures of a relativistic object using a time-stretch strategy", *Sci. Rep.*, vol. 5, p. 10330, 2015. doi:10.1038/srep10330

[33] L. Rota, C. M. Caselle, N. Hiller, A.-S. Mueller, and M. Weber, "An Ultrafast Linear Array Detector for Single-Shot Electro-Optical Bunch Profile Measurements", in *Proc. IBIC'14*, Monterey, CA, USA, Sep. 2014, paper TUPD10, pp. 435–437.